Title
Click by Click Microporous Annealed Particle (MAP) Scaffolds

Journal
Advanced Healthcare Materials, 9(10)

ISSN
2192-2640

Authors
Darling, Nicole J
Xi, Weixian
Sideris, Elias
et al.

Publication Date
2020-05-01

DOI
10.1002/adhm.201901391

Peer reviewed

Published in final edited form as:

Adv Healthc Mater. 2020 May ; 9(10): e1901391. doi:10.1002/adhm.201901391.

Click by Click Microporous Annealed Particle (MAP) Scaffolds

Nicole J. Darling,
Department of Chemical and Biomolecular Engineering, University of California Los Angeles, 420 Westwood Plaza, Los Angeles CA 90095

Weixian Xi,
Department of Chemical and Biomolecular Engineering, Department of Orthopedic Surgery, University of California Los Angeles, 420 Westwood Plaza, Los Angeles CA 90095

Elias Sideris,
Department Chemical and Biomolecular Engineering, University of California Los Angeles, 420 Westwood Plaza, Los Angeles CA 90095

Alexa R. Anderson,
Department of Biomedical Engineering, Duke University, 101 Science Drive Campus Box 90281, Durham NC 27708-0281, United States

Cassie Pong,
Department of Chemical and Biomolecular Engineering, University of California Los Angeles, 420 Westwood Plaza, Los Angeles CA 90095

S. Thomas Carmichael,
Department of Neurology, David Geffen School of Medicine, University of California Los Angeles, 621 Charles Young Drive, CA 90095, USA

Tatiana Segura*
Department of Biomedical Engineering, Duke University, 101 Science Drive Campus Box 90281, Durham NC 27708-0281, United States

Abstract

Macroporous scaffolds are being increasingly used in regenerative medicine and tissue repair. While our recently developed microporous annealed particle (MAP) scaffolds have overcome issues with injectability and *in situ* hydrogel formation, limitations with respect to tunability to be able to manipulate hydrogel strength and rigidity for broad applications still exist. To address these key issues, here we synthesized hydrogel microparticles (HMPs) of hyaluronic acid (HA) using the thiol-norbornene click reaction and then subsequently annealed HMPs into a porous scaffold using the tetrazine-norbornene click reaction. This assembly method allowed for straightforward tuning of bulk scaffold rigidity by varying the tetrazine to norbornene ratio, with increasing

*Corresponding author: tatiana.segura@duke.edu, Tel.: +1-919-660-2901.

Author contributions: N. J. D. and W. X. contributed equally to this work. N. J. D., W. X., E. S., and T.S. designed the experiments, N. J. D., W. X., E. S., A. R. A., and C. P. performed experiments and analyzed the results. N. J. D., W. X., A. R. A., and T.S. wrote the manuscript, with input from all authors. The authors would like to thank Dr. Talar Tokatlian for her assistance editing the manuscript.

Supporting Information

Supporting Information is available from the Wiley Online Library or from the author.

tetrazine resulting in increasing scaffold storage modulus, Young's modulus, and maximum stress. These changes were independent of void fraction. Further incorporation of human dermal fibroblasts (HDFs) throughout the porous scaffold revealed the biocompatibility of this annealing strategy as well as differences in proliferation and cell-occupied volume. Finally, injection of porous HA-Tet MAP scaffolds into an ischemic stroke model showed this chemistry is biocompatible *in vivo* with reduced levels of inflammation and astrogliosis as previously demonstrated for other crosslinking chemistries.

Keywords

Tetrazine; Norbornene; Porous Scaffold; Microbeads; Stroke

Granular hydrogels are materials generated from hydrogel microparticle (HMP) building blocks. A solution of HMPs can form a stable bulk gel when the HMPs are above a packing density of 0.58 and jamming can occur. In our laboratory, we crosslink HMPs to each other to generate a stable scaffold, rather than rely on jamming such that the void spaces surrounding the beads are sufficiently large for cellular growth and the scaffold is structurally stable. We termed these bulk hydrogels microporous annealed particle (MAP) scaffolds due to the micron sized voids (pores) formed in between packed beads. MAP scaffolds support modifications with bioactive ligands to modulate cell behavior, can be used for cell culture *in vitro*[1–8], and support tissue ingrowth *in vivo*[2–5]. Of particular interest is that injection of MAP scaffolds into wound sites results in reduced inflammation and improved tissue regeneration[3,4,9,10]. We have shown that the innate microporosity of MAP scaffolds enables a greater pro-repair response in the wound site after stroke compared to a nonporous gel of the same composition[5]. The 'plug and play' modularity of MAP building blocks enables the incorporation of different materials, signals, and crosslinking schemes to tune the scaffolds for unique tissue engineering applications. Herein, we demonstrate the generation of hyaluronic acid HMPs, the modification of HMPs with ligands, and the crosslinking of HMPs to form MAP scaffolds using thiol-norbornene and tetrazine-norbornene click reactions and their use *in vitro* and *in vivo.*

HMP interlinking to form MAP scaffolds can be achieved upon injection due to the shear thinning properties of these granular materials and the use of biocompatible mechanisms for annealing. Our current method to fabricate MAP scaffolds for use *in vivo* utilizes the coagulation enzyme FXIIIa, which is a transglutaminase[2,5,11]. The HMPs are packed and linked between K and Q peptides, recognized by FXIIIa, on their surface. For applications in wound healing, polyethylene glycol (PEG) HMPs annealed with FXIIIa *in situ* have been shown to promote cutaneous tissue regeneration by supporting cell migration and support tissue structure formation. *In vivo* responses to these injectable PEG MAP scaffolds include re-epithelialization, vascular development, and growth of hair follicles[2]. Utilizing the native extracellular matrix component hyaluronic acid (HA) with FXIIIa for scaffold fabrication accelerates brain repair processes after stroke[5]. Compared to both sham injections and nonporous gels, HA MAP reduces astroglyosis and inflammation while enhancing endogenous neural progenitor cell recruitment and vascularization in the peri-infarct cavity[5]. However, because the FXIIIa reaction is relatively inefficient, excess reagents are used for

this gelation scheme which results in poor control of crosslinking density between HMPs. Further, since the reaction is enzymatic, bond formation catalyzed by the enzyme can vary depending on environmental factors and enzyme activity. Thus, HMP linking to form a MAP scaffold cannot be easily tuned to modulate the strength and rigidity of the final scaffold. FXIIIa-crosslinked MAP typically has low storage modulus[2] and Young's modulus[12]. Biorthogonal click reactions pose as an attractive alternative to the existing annealing mechanism and have been increasingly utilized for hydrogel synthesis and functionalization for 3D cell culture and tissue engineering applications.[13–15] An alternative gelation approach to FXIIIa able to modulate scaffold mechanical properties would expand the application of MAP scaffolds for an array of tissue types. Here we explored a method to make MAP building blocks by using a thiol-norbornene click reaction to form HMPs and tetrazine-norbornene click reactions to anneal them to form Tet-MAP scaffolds.

Synthesis of Tet-MAP scaffolds using click by click reactions

Hyaluronic acid (HA) was modified to contain norbornene (HA-NB) groups through its carboxylic acid groups (Fig. 1A and materials and methods). NMR analysis shows that HA had 44% of its units modified with norbornene (Sup. Fig. 1). To generate the crosslinker, thiol-terminated polyethylene glycol (PEG) was modified with a maleimide-tetrazine bifunctional crosslinker (Fig. 1B and materials and methods,). NMR analysis shows 100% modification of PEG with tetrazine (Sup. Fig. 2). Fig. 1C introduces the two orthogonal click reactions that were used to generate HA-NB HMPs and Tet-MAP scaffolds (Fig. 1D). HMPs were generated using Thiol-ene Click chemistry occurring in an inverse suspension polymerization (Fig. 2A). Aqueous precursor solutions (HA-NB, dithriothreitol (DTT), Lithium phenyl-(2,4,6-trimethylbenzoyl)phosphinate (LAP)) were prepared and transferred to a continuous phase of hexane[16] with 3% Span-80 under nitrogen purge. In order to control microgel size, the solution was exposed to low shear through gentle pipetting and then maintained spinning at 600 rpm while UV light at 20 mW intensity initiated polymerization of the HMPs for 10 min. Particles were subsequently washed with hexane, swelled in 1% Pluronic in PBS, filtered through nylon mesh filters to gate various HMP ranges, and transitioned to PBS. The size distribution of the HMPs from each filter was characterized using an imageJ particle analyzer (Fig. 2B) and shown to have a mean diameter of 207.9 ± 48.21, 125.8 ± 35.51, and 76.59 ± 20.39 μm after passing through 200 μm, 100 μm, and 60 μm filters, respectively. As expected, HMP size distribution tightened as HMPs became further refined through sequential passes of decreasing filter size. The final HMPs have an HA-NB backbone crosslinked through a DTT nondegradable crosslinker.

Particles were synthesized with excess norbornene in the HA backbone to maximize the degree of functionalization for post-fabrication modification and annealing using tetrazine-functionalized small molecules and polymers. To model small molecule functionalization and render the HMPs fluorescent, tetrazine-modified Alexa Fluor molecules were synthesized (Tetrazine-Alexa488, Tetrazine-Alexa555, Tetrazine-Alexa647, Figure S3) and conjugated to HMPs post-fabrication (Fig. 2C). In this fashion, HMPs can be functionalized with different ligands post-HMP synthesis, which enables the generation of more sophisticated environments.

HA-NB HMP annealing to form MAP scaffolds was achieved using Tetra-PEG-Tet crosslinker (Fig. 1B, Figure S2). As expected, unannealed jammed HMPs display typical elastic hydrogel behavior with the storage modulus being larger than the loss modulus (G' > G") (Figure 2D). Upon crosslinker addition, the storage modulus drops due to the addition of liquid resulting in the HMP being less jammed (Fig. 2D). However, after crosslinking, the storage modulus of the scaffold increases beyond that of the unannealed HMPs (Fig. 2D). The kinetics of the crosslinking reaction were explored measuring G' over time at 1 Hz with 1% strain. G' increases with time for all the crosslinking ratios tested reaching a plateau. Annealing was shown to be dependent on temperature, requiring 60.5 min at 37°C to reach the plateau and 89.6 min at 25°C to reach the plateau (Fig. 2E). To investigate the effect of the number of links between HMPs on mechanical properties of the Tet-MAP scaffold, the degree of annealing was modulated by changing the moles of Tetrazine to moles of HA ratio (Tet/HA ratio) and analyzed via shear rheology and compression, to arrive at storage and Young's modulus, respectively. Increasing the crosslinker molar ratio increased the storage modulus of the gels from 278 Pa to 2016 Pa (Fig. 3A). Under compression, the modulus of the scaffold also increased with increasing Tet/HA ratio (Fig. 2B, C); in addition, the scaffold was able withstand more load with increasing Tet/HA ratio (Fig. 2C, right). Interestingly, under compression, jammed beads were unable to display elastic gel behavior with a flat stress strain curve (Fig. 2B, gray plot). These data show that tetrazine-norbornene chemistry allows for the tuning of the number of links between HMPs independent of HMP fabrication. Compared to our previous work with enzymatically annealed beads[12], tetra-PEG-Tet annealed MAP scaffolds display higher moduli (Fig. 2C, dash line), indicating stronger kinetics and more available crosslinking sites. Given that HMP could be further crosslinked by the Tetra-PEG-Tet, resulting in increased modulus of the HMP itself, we wanted to rule out that this alone could explain the differences observed in mechanical properties. We found that Tetra-PEG-Tet evenly diffuses approximately 20–25 μm into each bead and crosslinks it further for all of the Tet/HA ratios tested while the scaffold is annealing, (visualized by PEG-3Tet-Alexa555, Fig. S4). Given that the distance of crosslinking and intensity profile is similar for all conditions, the observed increase in bulk modulus for higher Tet/HA ratios is more likely a result of tighter connections between neighboring HMPs than the stiffening of individual beads.

To ensure tetrazine-norbornene annealed HMPs generated MAP scaffolds that remained porous, MAP scaffolds were labeled with 2,000 kDa fluorescein-labeled dextran solution to visualize pores (Fig. 4A). The dextran readily diffused throughout open pores but did not penetrate HMPs. IMARIS was used to quantify overall void space and determine there were no significant differences in void fraction across the various Tet/HA ratios (Fig. 4B), further indicating that the mechanical changes that were observed are dependent on the interconnections between HMPs.

Cell culture within tetrazine-norbornene annealed HA-MAP scaffolds

Given that the tetrazine-norbornene reaction results in the generation of one molecule of nitrogen, we wanted to ensure that this chemistry is biocompatible *in vitro* and *in vivo*. RGD-modified hyaluronic acid was used to generate HMPs. Following our previous protocols for culturing cells in MAP scaffolds, HMPs and cells (human dermal fibroblasts

(HDFs)) were mixed at a concentration of 2,000 cells/μL along with the Tetra-PEG-Tet crosslinker and allowed to anneal at 37°C. The kinetics of the crosslinker reaction are slow enough to allow sufficient mixing of the cells and HMPs to ensure even seeding. Overall cell viability was assessed with Live/Dead Kit (Invitrogen). The lowest and highest annealing ratios used, 2.5 and 20, showed high survival, >95%, for both Tet/HA annealing ratios at 1 day and 8-days post seeding (Fig 5A–C).

Post-encapsulation gels were fixed with 4% paraformaldehyde (PFA) (Fisher Scientific) for 15 minutes at room temperature after rinsing with 1xPBS. The cultures were permeabilized in 0.3% Triton X-100 in PBS and stained using Alexa Fluor 488 Phalloidin (1:40) (Invitrogen) for 90 minutes followed by 4',6-diamidino-2-phenylindole (DAPI) (1:500) (Sigma-Aldrich) for 10 minutes. The gels were washed with 1xPBS before 300 μm z-stacks were acquired on a Nikon-C2 laser scanning confocal microscope with a 20x air objective. The z-stacks were imported into IMARIS to generate Spot models of DAPI channel, surface renders of F-actin channel, and quantify the occupied volume of cells. Using these methods, we further assess biocompatibility using long term culture with 2.5 Tet/HA annealing ratio. HDFs showed significant proliferation over time (Fig. 5C) and degree of cell spreading (Fig. 5B), showing that the chemistry does not negatively impact cell growth long term. The number of cells increased by approximately 3-fold at two weeks relative to the average of all day 2 nuclei counts as quantified by IMARIS Spot modeling of the DAPI channel (Fig. 5D). HDF cell spreading was assessed at 2, 5, and 14-days via confocal microscopy and subsequent surface renderings in IMARIS to quantify volume of F-actin. Both the degree of spreading and number of cells increased with time (Fig. 5E). By day 2, significant cell spreading was observed, which occurred within the void space of the MAP scaffold (Fig. 5F). IMARIS 3D rendering of the cells over time (Fig. 5G) as well as the cells and scaffold (Fig. 5H) show again that in the volume of the scaffold, the cells reside in the interstitial space and that the cell number increases over time.

From our viability experiment it appeared that HDFs spread more in the 2.5 versus 20 Tet/HA ratio gels. Since the viability of the scaffold is the same for both conditions, we further investigated the effect of HMP annealing degree on spreading and proliferation. Cell-loaded MAP scaffolds were generated with 2.5, 5, 10, or 20 Tet/HA ratio and analyzed for cell spreading, cell metabolic activity, and overall cell volume at 2 and 5-days post seeding. Cells were able to spread in all the scaffolds as determined by F-actin staining and confocal microscopy imaging (Fig. 5I). Analysis of the occupied volume via IMARIS 3D analysis software reveals that cells seeded in 2.5 Tet/HA ratio scaffolds contain more cell volume than cells in the other Tet/HA ratio scaffolds for all the time points tested (Fig. 5K). The percent of occupied cell volume increases for all Tet/HA scaffolds between days 2 and 5 post-encapsulation, with noticeable increases in cell spreading for Tet/HA ratios of 2.5 and 5. Analysis of metabolic activity with the PrestoBlue assay (Thermo Fisher) at 2 and 5-days, revealed that cells seeded in 2.5 and 5 Tet/HA ratio scaffolds resulted in a higher proliferation rate compared to 10 and 20 Tet/HA (Fig. 5L,M). Taken together these data indicate that cells seeded on stiffer scaffolds generated by the 10 and 20 Tet/HA crosslinker ratio result in significantly less cell spreading and proliferation.

In vivo biocompatibility of Tet-MAP scaffolds in brain tissue

We next assessed the biocompatibility of tetrazine-norbornene crosslinkers *in vivo*. We chose to inject the material into a brain wound environment because it is an environment with an increased population of immune cells and because of our interest in stroke repair. We have previously shown that hydrogels can be injected into the stroke core without damaging the brain or causing swelling[5,17–19]. The peri-infarct space, region that surrounds the stroke core, is the tissue of the brain that undergoes the most substantial repair post-stroke[17]. Thus, injecting material into the stroke core itself provides an opportunity to develop regenerative tissue engineering therapies promote brain repair post-stroke. Previous work in our lab from Nih and Sideris showed that the use of HA-MAP gels annealed by FXIIIa were biocompatible and resulted in less microglia infiltration and astrocytic scarring compared to a nonporous hydrogel of the same biochemical composition[5]. Here we aimed to assess the effect, if any, of using the tetrazine-norbornene reaction for HMP annealing to form *in situ* MAP scaffolds in the brain. In our experimental timeline, a photothrombotic stroke is induced in the motor cortex at t = 0 and five days (t = 5-days) later a gel is injected at the same coordinates where the stroke was induced (Fig. 6A). Five days after stroke, the stroke core is surrounded by an astrocytic scar (Fig. 6B). Microphage/microglia are observed both inside the stroke core and in the surrounding peri-infarct tissue (Fig. 6B). Following hydrogel injection, no obvious damage to the surrounding brain tissue was observed (Fig. 6C). Similar to FXIIIa-crosslinked HA-MAP scaffolds, we found that tetrazine-norbornene crosslinked HA-MAP (Tet-MAP) scaffolds reduced the number of inflammatory monocytes (CD11b+) cells (Fig. 6D). Quantification of the infarct and peri-infarct region for CD11b+ area (Fig. 6E) reveals that the area covered by CD11b+ cells is statistically lower for animals treated with Tet-MAP gel (Fig. 6F). The observed reduction of monocytes in response to tetrazine-norbornene crosslinked HA-MAP scaffolds suggests an overall decrease in inflammation and is supported by our previous finding that HA-MAP injection into the stroke cavity using an alternative chemistry for annealing upregulate Arginase-1+ macrophages, which corresponds to a pro-reparative, anti-inflammatory phenotype[20]. Analysis of the astrocytic scar again revealed that similar to FXIIIa crosslinked HA-MAP scaffolds, injection of Tet-MAP into the stroke core visibly reduced astrocytic scar thickness (Fig. 6G). Quantification of the scar thickness (Fig. 6H) revealed statistical significance for thickness reduction with Tet-MAP compared to sham groups (Fig. 6I). Together these data show that tetrazine-norbornene chemistry can be used as a crosslinker *in vivo* without causing more inflammation or reactive astrogliosis.

Conclusion

Tet-MAP scaffolds crosslinked using click-by-click chemistry were developed to be able to easily tune material properties for the study of cell behavior *in vitro* and for therapeutic use *in vivo*. By manipulating the Tet/HA annealing ratio, we were able to tune the rigidity of the scaffold which influenced how HDFs behave within the porous scaffold. In particular, we observe that MAP scaffolds containing lower annealing degree allowed cells to proliferate faster and result in substantial cell spreading compared to MAP scaffold that contained a higher annealing degree, likely due to the ability of cells to re-arrange their local environment in a less crosslinked, less stiff scaffold. Further, we find that tetrazine-

norbornene chemistry is biocompatible *in vivo* using an experimental ischemic stroke model in mice with our results mirroring what we observed for HMPs crosslinked with factor XIIIa enzyme. In particular, we found that *in situ* annealing of HMPs to form MAP scaffolds in the stroke cavity lowers the CD11b+ cell population and decreases the scar thickness surrounding the stroke. This platform holds potential to investigate how different HMP properties like size, shape, mechanical strength, topography/porosity, and biochemical composition impact cellular responses and tissue repair.

Experimental Section:

Synthesis of Tetrazine Reactive Monomers:

Tetra-polyethylene glycol-tetrazine (Tetra-PEG-Tet) was synthesized through a base-catalyzed thiol-Michael addition by dissolving 100 mg of tetra-PEG-SH (MW: 20,000 Da) (NOF America, White Plains, NY) and 15 mg of methyltetrazine-PEG4-maleimide (MW: 514.53 Da) (Kerafast, Boston, MA) in 0.5 mL $CDCl_3$ (maleimide/SH ratio of 1.05), then adding 1 μL of triethylamine (TEA) (0.5 molar equivalent). (**Scheme 1B**) The mixture was stirred at room temperature for 4 hrs. The product was precipitated in 50 mL cold diethyl ether and confirmed by ^{1}H-NMR with 98% conversion (Figure S2).

Alexa Fluor 647 C2-tetrazine (Alexa647-Tet) was synthesized through two base-catalyzed thiol-Michael addition reactions in series. (Figure S3) First, by dissolving 2.8 mg of HS-PEG-SH (MW: 3500 Da) (JenKem Technology USA, Plano, TX) (1 molar equivalent to Alexa Fluor C2 maleimide) and 0.41 mg of methyltetrazine-PEG4-maleimide (MW: 514.53 Da) (Kerafast, Boston, MA) (1 molar equivalent to Alexa Fluor C2 maleimide) in 0.17 mL $CDCl_3$, then adding 0.11 μL of triethylamine (TEA) (0.5 molar equivalent). The mixture was stirred at room temperature overnight. Next, by dissolving 1 mg Alexa Fluor 647 C2 maleimide (MW: 1250 Da) (Thermo Fisher Scientific) in 0.17 mL $CDCl_3$, then adding the reaction mixture and 0.11 μL of triethylamine (TEA) (0.5 molar equivalent). The mixture was stirred at room temperature overnight. The product was precipitated in 10 mL of cold diethyl ether and dried under vacuum overnight. The resulting product was dissolved in dimethylformamide at 1 mg/mL and stored at −20°C.

μbead Modification:

HA-Norb HMP were modified post-fabrication via inverse electron demand Diels-Alder tetrazine-norbornene click reaction, in which excess norbornene groups on the HMP were functionalized with Alexa647-Tet to fluorescently tag the HMP. Briefly, the HMP were incubated in 1xPBS containing a final Alexa647-Tet concentration of 0.005 mM at 37°C for 1 hour under agitation (i.e. 200 μL of HMP were combined with 100 μL 1xPBS containing 0.015 mM Alexa647-Tet (1:13 dilution of the 1 mg/mL Alexa647-Tet stock)). Upon completion of the functionalization, the suspended HMP were pelleted by centrifuging at 14,000 rcf for 5 minutes. The HMP were washed three times with 1xPBS and recovered with the same centrifugation conditions. The labeled HMP were stored at 4°C until further use.

Tet-MAP Scaffold Assembly:

Macroporous annealed particle (MAP) scaffolds were assembled via inverse electron demand Diels-Alder tetrazine-norbornene click reaction, in which excess norbornene groups on the HMP were linked by tetra-PEG-Tet to form tetrazine mediated MAP (Tet-MAP) scaffolds. The theoretical HA-Norb concentration (0.18 mM) in a volume of pelleted HMP was first calculated by converting the total μbead weight percent, determined by lyophilizing 100 μL of unlabeled HMP to get the total mass, using the mass fractions of the μbead contents. This theoretical concentration was then used to determine the final tetra-PEG-Tet annealing concentrations: 0.11 mM, 0.22 mM, 0.44 mM, and 0.89 mM for tetrazine/HA-Norb (Tet/HA) ratio of 2.5, 5, 10, and 20. The volume of tetra-PEG-Tet added to the HMP was consistent across the four Tet/HA conditions, 5/6 of the final Tet-MAP scaffold volume was HMP and 1/6 of the volume was concentrated tetra-PEG-Tet (0.22 mM, 0.45 mM, 0.89 mM, and 1.79 mM, respectively). Tet-MAP scaffolds were formed by combining and mixing HMP with concentrated tetra-PEG-Tet at the desired Tet/HA ratio and incubated for 1 hour at 37°C unless stated otherwise. All Tet-MAP scaffolds were formed using the 60 – 100 μm bead size filter range.

Animal Stroke Model, Tissue Processing, Immunohistological Staining and Image Analysis:

Animal procedures were performed in accordance with the US National Institutes of Health Animal Protection Guidelines and the University of California Los Angeles Chancellor's Animal Research Committee. The stroke model was performed as previously described. Briefly, a permanent cortical photothrombotic stroke was induced on young adult C57BL/6 male mice (8–12 weeks) obtained from Jackson laboratories (Bar Harbor, ME). The mice were anesthetized with 5% isoflurane and placed in a stereotactic setup. The mice were kept at 2.5% isoflurane in N2O:O2 for the duration of the surgery. A midline incision was made and Rose Bengal (10 mg/mL, Sigma-Aldrich) was injected intraperitoneally at 10 μL/g of mouse body weight. After 5 minutes, a 2-mm diameter cold fiberoptic light source was centered at 0 mm anterior/1.5 mm lateral left of the bregma for 18 minutes and a burr hole was drilled through the skull in the same location. All mice were given sulfamethoxazole and trimethoprim oral suspension (TMS, 303 mL TMS/250 mL H20, Amityville, NY) every 5 days for the entire length of the experiment.

Five days post-stroke, freshly mixed HMP with concentrated tetra-PEG-Tet at a Tet/HA ratio of 5 was loaded into a 25 μL Hamilton syringe (Hamilton Reno, NV) connected to a pump and 6 μL of microgels were injected into the stroke cavity using a 30 gauge needle at a depth of 0.8 mm and the same stereotaxic coordinates as above at an infusion speed of 1 μL/min. The needle was withdrawn from the mouse brain 5 min after the injection to allow for annealing of the Tet-MAP scaffold.

Ten days post-injection, mice were sacrificed via transcardial perfusion of 1xPBS followed by 40 mL of 4% PFA. The brains were isolated and post-fixed in 4% PFA overnight and submerged in 30 (w/v) % sucrose solution for 48 h. Tangential cortical sections of 30 μm thickness were sliced using a cryostat and directly mounted on gelatin-subbed glass slides. Slides not immediately stained were kept at −80°C.

Each slide was rinsed with 1xPBS for 10 minutes at room temperature, dried and outlined with a hydrophobic pen (ImmEdge Hydrophobic Barrier PAP Pen, Vector Labs). The slides were then incubated in a blocking solution containing 1xPBS, 0.3% Triton X-100 and 10% normal donkey serum for 1–2 h at room temperature. The slides were then incubated in the primary antibody at the appropriate dilution in blocking solution overnight at 4°C. After 3× 10 minute washes in 1x PBS, the slides were incubated in the secondary antibodies at the appropriate dilution in blocking solution for 2 hours at room temperature. The slides were then counterstained with the nuclear marker DAPI (1:500, Invitrogen) for 15 minutes at room temperature. After allowing the slides to dry at room temperature after 3× 10 minute washes in 1xPBS, the slides were dehydrated in ascending ethanol baths, incubated in xylene and mounted in mounting medium (DPX, Sigma-Aldrich). Primary antibodies were used as follows: rat anti-glial fibrillary acidic protein (GFAP, 1:100, Abcam, Cambridge, MA, USA) for astrocytes and rat anti-CD11b (1:100, Abcam, Cambridge, MA, USA) for microglial and macrophage cells. Secondary antibodies, matching the desired primary antibody host, conjugated to Alexa Fluor 488 (1:500, Jackson Immuno Research, West Grove, PA) were used. A Nikon-C2 laser scanning confocal microscope with a 20x air objective used to take fluorescent images represented as maximum intensity projections.

Analyses were performed on microscope images of three coronal brain levels at +0.80, −0.80, and −1.20 mm according to bregma, which consistently contained the cortical infarct area. The thickness of scar was measured on the ischemic boundary zone within the ipsilateral hemisphere on three sections stained for GFAP. The astrocytic (GFAP) infiltration into the stroke cavity was measured in ImageJ as the shortest distance from a $GFAP^+$ cell to the ischemic boundary zone. The inflammation (CD11b) positive area in the infarct and peri-infarct areas were quantified using ImageJ and expressed as the area fraction of positive signal per total area (%). All measurements were averaged across sections and presented per animal.

Statistical Analysis:

Pre-processing of data included normalization of cell nuclei to day 2 nuclei counts. Data are presented error bars representing standard error of the mean. For *in vitro* experiments, n = 3 for gels of each Tet/HA ratio unless specified otherwise. Three regions of interest from one Z-stack for each Tet/HA ratio were analyzed for occupied cell volume and nuclei counts. One-way ANOVA performed for the following: percent occupied volume, relative proliferation, storage moduli, Young's moduli, and max stress yielded $P<0.05$ prompting post-hoc analysis. Tukey's multiple comparison test was used to compare groups defined by Tet/HA ratio. One-way ANOVA analysis of void fraction for varying Tet/HA yielded $P>0.05$; therefore, post-hoc analysis was not conducted. For *in vivo* experiments, n=5 unless specified otherwise, where n represents the number of animals. Signal measurements were averaged across sections and presented per animal. Two-tailed unpaired t-test with Welch's correction was used to compare staining of No Gel versus Tet-MAP groups. For all experiments, significance is indicated by * $P<0.05$, ** $P<0.01$, *** $P<0.001$, **** $P<0.0001$. GraphPad Prism was used to conduct statistical analysis.

Supplementary Material

Refer to Web version on PubMed Central for supplementary material.

References

1. Caldwell AS, Campbell GT, Shekiro KMT & Anseth KS Clickable Microgel Scaffolds as Platforms for 3D Cell Encapsulation. Adv Healthc Mater 6, doi:10.1002/adhm.201700254 (2017).
2. Griffin DR, Weaver WM, Scumpia PO, Di Carlo D & Segura T Accelerated wound healing by injectable microporous gel scaffolds assembled from annealed building blocks. Nat Mater 14, 737–744, doi:10.1038/nmat4294 (2015). [PubMed: 26030305]
3. Hsu R-S et al. Adaptable Microporous Hydrogels of Propagating NGF-Gradient by Injectable Building Blocks for Accelerated Axonal Outgrowth. Advanced Science 0, 1900520, doi:10.1002/advs.201900520.
4. Mealy JE et al. Injectable Granular Hydrogels with Multifunctional Properties for Biomedical Applications. Adv Mater 30, e1705912, doi:10.1002/adma.201705912 (2018). [PubMed: 29602270]
5. Nih LR, Sideris E, Carmichael ST & Segura T Injection of Microporous Annealing Particle (MAP) Hydrogels in the Stroke Cavity Reduces Gliosis and Inflammation and Promotes NPC Migration to the Lesion. Adv Mater 29, doi:10.1002/adma.201606471 (2017).
6. Truong NF, Lesher-Perez SC, Kurt E & Segura T Pathways Governing Polyethylenimine Polyplex Transfection in Microporous Annealed Particle Scaffolds. Bioconjug Chem 30, 476–486, doi:10.1021/acs.bioconjchem.8b00696 (2019). [PubMed: 30513197]
7. Xin S, Chimene D, Garza JE, Gaharwar AK & Alge DL Clickable PEG hydrogel microspheres as building blocks for 3D bioprinting. Biomaterials science, doi:10.1039/c8bm01286e (2019).
8. Xin S, Wyman OM & Alge DL Assembly of PEG Microgels into Porous Cell-Instructive 3D Scaffolds via Thiol-Ene Click Chemistry. Adv Healthc Mater 7, e1800160, doi:10.1002/adhm.201800160 (2018). [PubMed: 29663702]
9. Nih LR, Sideris E, Carmichael ST & Segura T Injection of Microporous Annealing Particle (MAP) Hydrogels in the Stroke Cavity Reduces Gliosis and Inflammation and Promotes NPC Migration to the Lesion. Advanced Materials 29, doi:ARTN 1606471 10.1002/adma.201606471 (2017).
10. Griffin DR, Weaver WM, Scumpia PO, Di Carlo D & Segura T Accelerated wound healing by injectable microporous gel scaffolds assembled from annealed building blocks. Nature materials, doi:10.1038/nmat4294 (2015).
11. Koh J et al. Enhanced In Vivo Delivery of Stem Cells using Microporous Annealed Particle Scaffolds. Small, e1903147, doi:10.1002/smll.201903147 (2019). [PubMed: 31410986]
12. Sideris E et al. Particle Hydrogels Based on Hyaluronic Acid Building Blocks. Acs Biomater Sci Eng 2, 2034–2041, doi:10.1021/acsbiomaterials.6b00444 (2016).
13. Xi WX, Scott TF, Kloxin CJ & Bowman CN Click Chemistry in Materials Science. Adv Funct Mater 24, 2572–2590, doi:10.1002/adfm.201302847 (2014).
14. Alge DL, Azagarsamy MA, Donohue DF & Anseth KS Synthetically Tractable Click Hydrogels for Three-Dimensional Cell Culture Formed Using Tetrazine-Norbornene Chemistry. Biomacromolecules 14, 949–953, doi:10.1021/bm4000508 (2013). [PubMed: 23448682]
15. Azagarsamy MA & Anseth KS Bioorthogonal Click Chemistry: An Indispensable Tool to Create Multifaceted Cell Culture Scaffolds. Acs Macro Lett 2, 5–9, doi:10.1021/mz300585q (2013). [PubMed: 23336091]
16. Yang C, Tibbitt MW, Basta L & Anseth KS Mechanical memory and dosing influence stem cell fate. Nature materials 13, 645–652, doi:10.1038/nmat3889 (2014). [PubMed: 24633344]
17. Lam J, Lowry WE, Carmichael ST & Segura T Delivery of iPS-NPCs to the Stroke Cavity within a Hyaluronic Acid Matrix Promotes the Differentiation of Transplanted Cells. Adv Funct Mater 24, 7053–7062, doi:10.1002/adfm.201401483 (2014). [PubMed: 26213530]
18. Moshayedi P et al. Systematic optimization of an engineered hydrogel allows for selective control of human neural stem cell survival and differentiation after transplantation in the stroke brain. Biomaterials 105, 145–155, doi:10.1016/j.biomaterials.2016.07.028 (2016). [PubMed: 27521617]

19. Nih LR, Gojgini S, Carmichael ST & Segura T Dual-function injectable angiogenic biomaterial for the repair of brain tissue following stroke. Nat Mater, doi:10.1038/s41563-018-0083-8 (2018).

20. Sideris E, Yu A, Chen J Carmichael ST, & Segura T Hyaluronic acid particle hydrogels decrease cerebral atrophy and promote pro-reparative astrocyte/axonal infiltration in the core after ischemic stroke. bioRxiv, 768291 doi:10.1101/768291doi (2019).

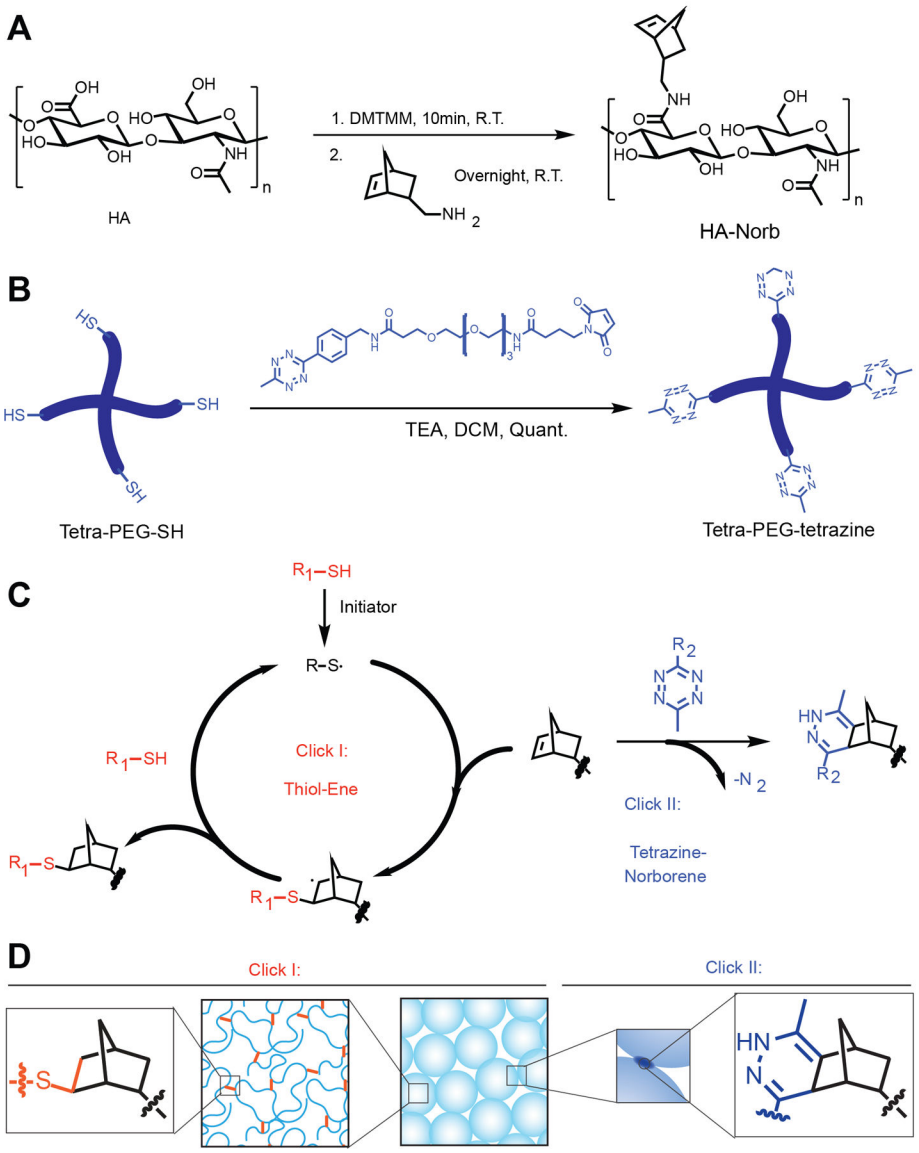

Figure 1.

Schematic overview for the HA backbone modification, HMP crosslinker synthesis, and the click by click chemistry for both generating and annealing HMPs. (A) Hyaluronic acid-norbornene (HA-NB) was synthesized through the activation and subsequent functionalization of the HA carboxylic acid group. (B) Tetra-polyethylene glycol-tetrazine (Tetra-PEG-Tet) was synthesized through a base-catalyzed thiol-Michael addition for the purpose of annealing beads. (C) Click I is described as the radical-mediated step-growth thiol-norbornene photo-click reaction, and Click II is the tetrazine-norbornene cycloaddition click reaction. Graphical depictions of the click by click chemistry are shown in (D)for forming HMPs using thiol-norbornene (Click I) as well as annealing HMPs using tetrazine-norbornene click chemistry (Click II) to generate MAP scaffolds.

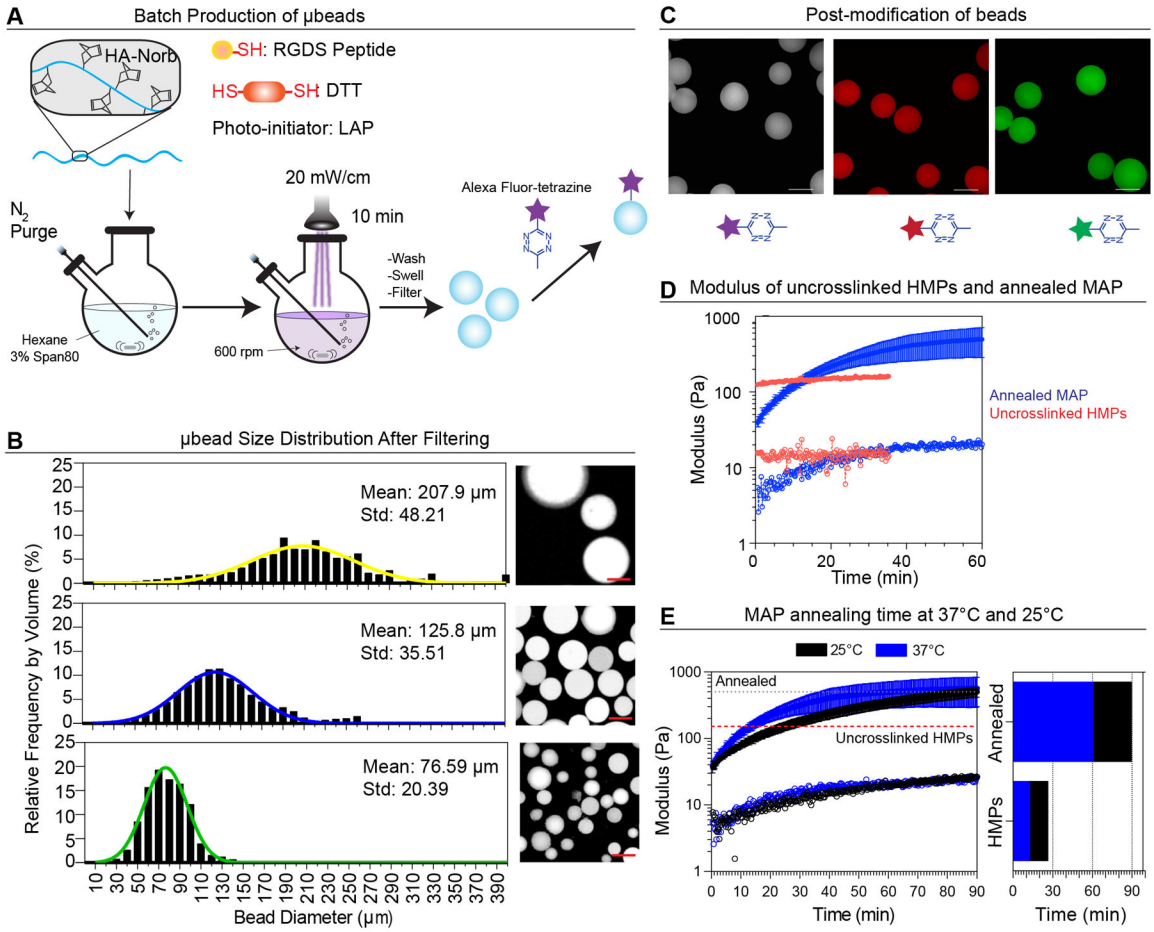

Figure 2.

Synthesis and characterization of µbead building blocks and annealing of Tet-MAP scaffolds. (A) Overview schematic of the µbead fabrication and purification. Final bead preparations were sequentially filtered through decreasing size filters to control for µbead size. A representative image of Alexa FluorTetrazine fluorescently labeled HMPs within each filtered range is depicted. Scale bars = 100 µm. (B) Relative frequency by volume of µbead diameter was treated as Gaussian distribution showing mean diameter of 207.9 ± 48.21µm, 125.8 ± 35.51µm, and 76.59 ± 20.39µm for the 200–100 µm, 100–60 µm, and 60–20 µm filter ranges. Greater than or equal to 1000 HMPs were analyzed in each range. All HMP used were from the 100–60 µm filter range. (C) Fluorescent labeling can be performed after HMP formation by post-modifying with Alexa Fluor-Tetrazine (D) Time sweep of Tet-MAP scaffold with Tet/HA ratio of 10 (blue) compared to uncrosslinked HMPs (red). (E) Additionally, Tetra-PEG-Tet was added to the packed HMPs and the G' of Tet-MAP at 37°C (blue) and 25°C (red) was monitored over time. The red dashed line represents the G' of packed HMPs without crosslinker. The grey dashed line represents G' at plateau once the HMPs have annealed to form the MAP scaffold. The Tet-MAP scaffold crossed the uncrosslinked HMPs line at 12.6 min and 26.4 min and the Annealed line at 60.5 min and 89.6 min, respective to each temperature.

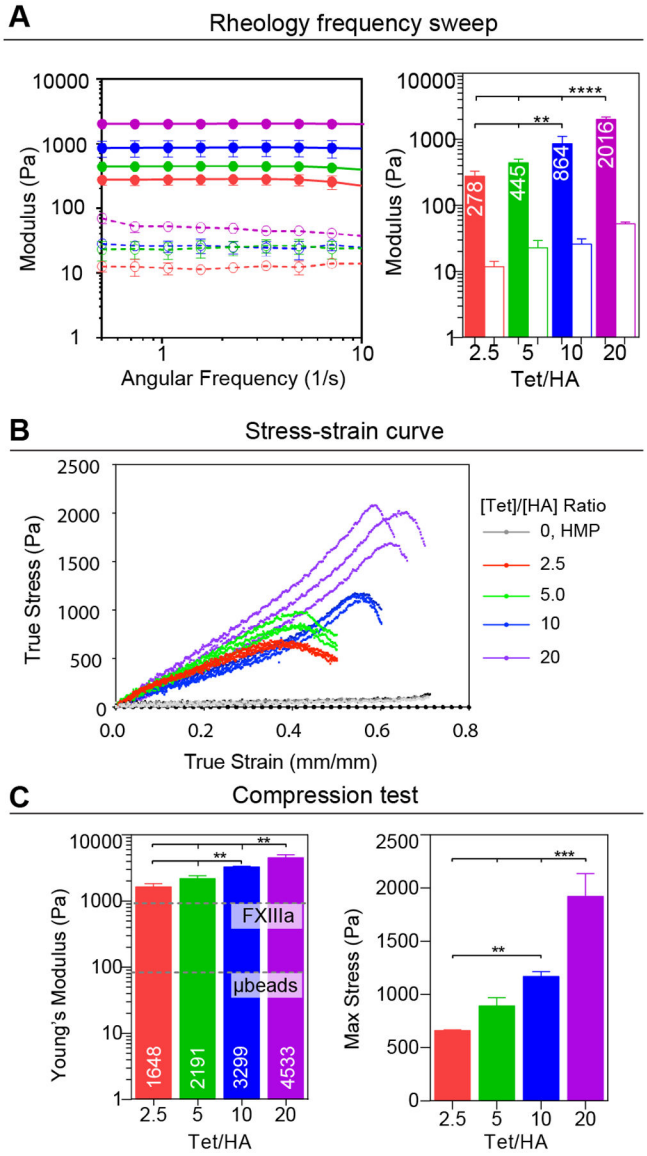

Figure 3.

Characterization of Tet-MAP scaffolds with 2.5, 5, 10, and 20 Tet/HA ratios. (A) Frequency sweeps describing storage (solid circles/bars) and loss (open circles/bars) modulus. (B) Stress-strain curve for Tet-MAP scaffolds compared to packed HMPs. (C) Young's modulus (FXIIIa line represents MAP annealed using previously reported K peptide, Q peptide and FXIIIa; µbead line represents packed HMP only and max stress for each Tet/HA ratio. One-way ANOVA performed for storage moduli, Young's moduli, and max stress yielded $P<0.05$ prompting post-hoc analysis with Tukey's multiple comparison test (significance indicated by * $P<0.05$, ** $P<0.01$, *** $P<0.001$, **** $P<0.0001$). For all experiments, n = 3 for gels of each Tet/HA ratio unless specified otherwise.

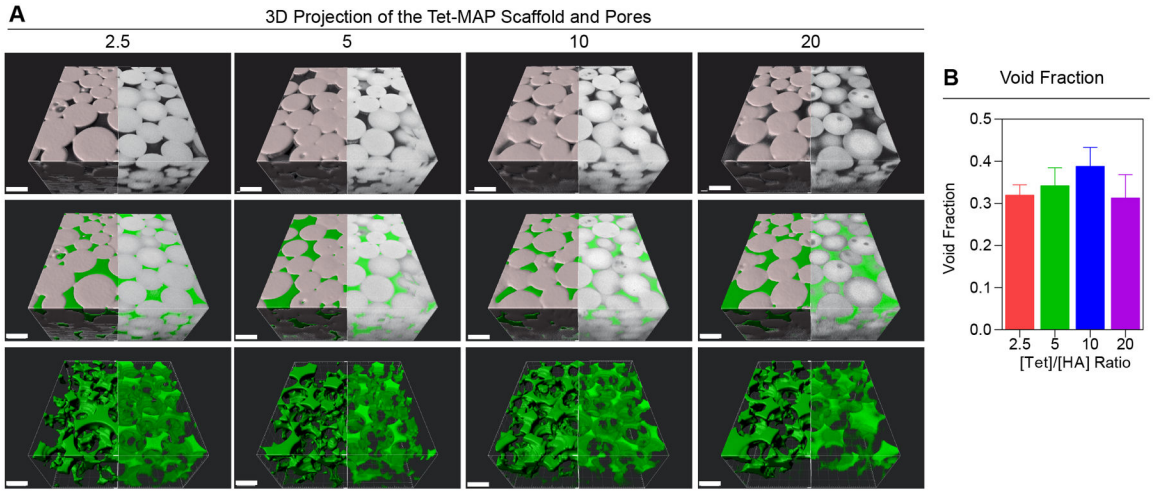

Figure 4.

Representative images of Tet-MAP scaffolds with 2.5, 5, 10, 20 Tet/HA annealing ratios. (A) IMARIS was used to generate renderings of 300 μm z-stacks. The model generated from raw data is depicted on the left half of each image and the raw data is depicted on the right half of each image. μbeads are shown in white and the void (filled with 2,000 kDa FITC-dextran) is shown in green; scale bars = 200μm. (B) Void fraction (computed using IMARIS) of Tet-MAP scaffolds with 2.5, 5, 10, and 20 Tet/HA ratios with error bars representing standard error of the mean. One-way ANOVA analysis of void fraction for varying Tet/HA yielded $P>0.05$; therefore, post-hoc analysis was not conducted. For all experiments, $n = 3$ for gels of each Tet/HA ratio unless specified otherwise.

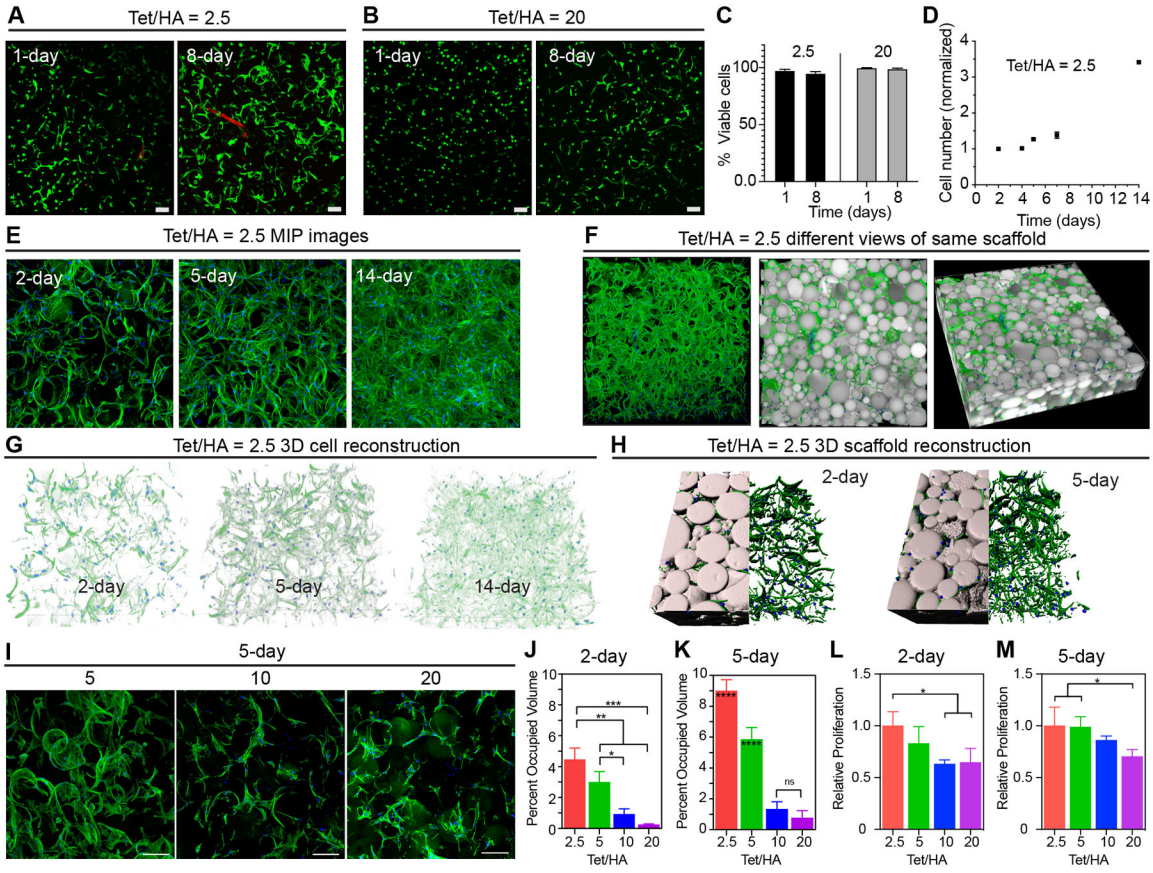

Figure 5.

In vitro cellular response to Tet-MAP scaffolds. (A) Representative images and analysis of HDFs (F-actin labeled green) in Tet-MAP scaffolds 1 and 8-days post-encapsulation with Tet/HA annealing ratios of (A) 2.5 and (B) 20. (C) Overall cell viability was assessed with the lowest and highest annealing ratios used, 2.5 and 20, and showed high survival (>95%) for both Tet/HA annealing ratios at 1 day and 8-days post-encapsulation. (D) The number of cells relative to the average of all day 2 nuclei counts. (E) Representative maximum intensity projection (MIP) images of HDFs in 2.5 Tet/HA scaffolds 1 and 8-days post-encapsulation. (F) 3D projection of the 300 μm z-stacks with HMPs shown in white, F-actin shown in green, and cell nuclei (labeled with DAPI) are shown in blue. (G) IMARIS analysis of HDF nuclei in z-stacks to obtain information about cell number and proliferation (H) IMARIS renderings of confocal microscopy z-stacks. The model generated from raw data is depicted on the left half of each image and the raw data is depicted on the right half of each image. (I) Cells were able to spread in all the scaffolds as determined by phalloidin staining and confocal microscopy imaging. The percent volume occupied by HDFs F-actin measured by IMARIS at three different regions in a scaffold of each Tet/HA on (J) 2 days and (K) 5 days post-encapsulation. Relative proliferation measured by PrestoBlue at (L) 2 days and (M) 5 days. One-way ANOVA performed for percent occupied volume and relative proliferation yielded $P<0.05$ prompting post-hoc analysis with Tukey's multiple comparison test (significance indicated by * $P<0.05$, ** $P<0.01$, *** $P<0.001$, **** $P<0.0001$). For all experiments, n = 3 for gels of each Tet/HA ratio unless specified otherwise.

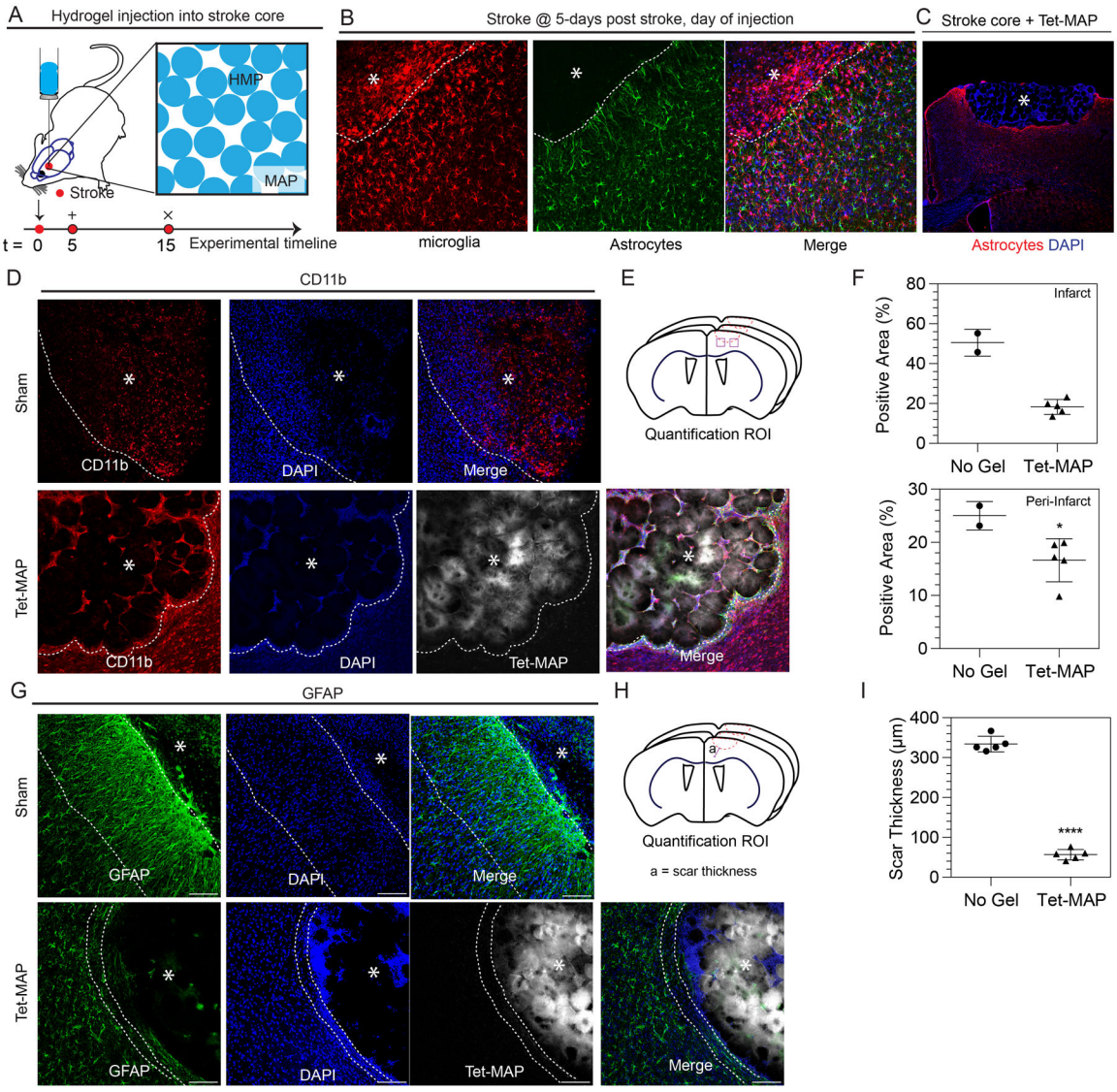

Figure 6.

In vivo cellular response to Tet-MAP scaffold in a PT stroke model. (A) Overview schematic of PT stroke timeline and stroke injection concept. (B) Images showing the microglia/macrophage (IBA1) and astrocytic (GFAP) response at 5-days post stroke, which is the day of hydrogel injection. (C) Image showing brain + Tet-MAP at 2-weeks post stroke. The gel area completely fills the stroke core. Fluorescent images at 2-weeks of (D) CD11b staining showing the post-stroke microglial response. (E) The ROI for quantification is highlighted in for (F) analysis of CD11b+ area in both the infarct and peri-infarct regions. (G) GFAP staining showing the post-stroke astrocyte response and (H) the ROI for quantification of GFAP+ response in terms of scar thickness (I). Scale bars = 100µm; white star indicates the infarct region. Two-tailed unpaired t-test with Welch's correction was used to compare staining of No Gel versus Tet-MAP groups (significance indicated by * P<0.05, ** P<0.01,

*** P<0.001, **** P<0.0001). (n = 5 unless specified otherwise, where n represents the number of animals)